Mon. Not. R. Astron. Soc. **321**, 487–496 (2001)

Morphological and kinematic signatures of a binary central star in the planetary nebula Hu 2-1

Luis F. Miranda,[1★] José M. Torrelles,[2★] Martín A. Guerrero,[3★] Roberto Vázquez[4★] and Yolanda Gómez[5★]

[1]*Instituto de Astrofísica de Andalucía, CSIC, Apdo. Correos 3004, E-18080 Granada, Spain*
[2]*Institut d'Estudis Espacials de Catalunya (IEEC/CSIC) and Instituto de Ciencias del Espacio (CSIC), Edifici Nexus, C/ Gran Capitá 2-4, E-08034 Barcelona, Spain*
[3]*Department of Astronomy, University of Illinois at Urbana-Champaign 1002 West Green Street, Urbana, IL 61801, USA*
[4]*Instituto de Astronomía, UNAM, Apto. Postal 877, 22800 Ensenada, B.C., México*
[5]*Instituto de Astronomía UNAM, Campus Morelia, A.P. 3-72 (Xangari), c.p. 58089 Morelia, Michoacán, México*

Accepted 2000 September 15. Received 2000 September 7; in original form 2000 April 5

ABSTRACT

We present Hα, [N II] and [O III] ground-based and *HST* archive images, VLA–A 3.6-cm continuum and H92α emission-line data and high-resolution long-slit [N II] spectra of the planetary nebula Hu 2-1. A large number of structural components are identified in the nebula: an outer bipolar and an inner shell, two pairs of collimated bipolar structures at different directions, monopolar bow-shock-like structures, and an extended equatorial structure within a halo. The formation of Hu 2-1 appears to be dominated by anisotropic mass ejection during the late-AGB stage of the progenitor and by variable, 'precessing' collimated bipolar outflows during the protoplanetary nebula and/or early planetary nebula phases. Different observational results strongly support the existence of a binary central star in Hu 2-1, among them (1) the observed point-symmetry of the bipolar lobes and inner shell, and the departures from axial symmetry of the bipolar lobes, (2) the off-centre position of the central star, (3) the detection of mass ejection towards the equatorial plane, and (4) the presence of 'precessing' collimated outflows. In addition, (5) an analysis of the kinematics shows that the systemic velocity of the bipolar outflows does not coincide with the systemic velocity of the bipolar shell. We propose that this velocity difference is a direct evidence of orbital motion of the ejection source in a binary system. From a deduced orbital velocity of $\sim$10 km s^{-1}, a semimajor axis of $\sim$9–27 au and period of $\sim$25–80 yr are obtained, assuming a reasonable range of masses. These parameters are used to analyse the formation of Hu 2-1 within current scenarios of planetary nebulae with binary central stars.

Key words: stars: mass-loss – ISM: jets and outflows – ISM: kinematics and dynamics – planetary nebulae: individual: Hu 2-1.

1 INTRODUCTION

Binary stars are emerging as a basic ingredient in the formation and evolution of many planetary nebulae (PNe). Binary scenarios, involving different kinds of systems, have been invoked to provide qualitative explanations for different observations including, among others, the common asphericity of the PN shells and the existence of collimated outflows in PNe (e.g. Morris 1987; Soker & Livio 1994; Soker 1996; Mastrodemos & Morris 1998, 1999). On the other hand, only a small number of wide (separation $\sim 10^2$–10^4 au, period $\sim 10^3$–10^6 yr) and close (separation $\sim$1–35 R$_\odot$, period $\sim$0.11–16 d) binary central stars are presently known (Ciardullo et al. 1999; Soker 1999; Bond 2000, and references therein), most likely because direct detection is severely hampered by the present instrumental resolution, the nature of the binary itself and/or of its (stellar or substellar) companion, and even by the evolution of the system (i.e., the binary may not exist anymore; e.g. Soker 1996). Therefore a reasonable alternative to infer the possible presence and properties of a binary central star is to search for the influence of binary evolution in the nebular properties (e.g. Soker 1998).

Hu 2-1 (PN G051.4+09.6) is a young PN whose properties

★ E-mail: lfm@iaa.es (LFM); torrelles@ieec.fcr.es (JMT); mar@astro.uiuc.edu (MAG); vazquez@astrosen.unam.mx (RV); gocy@astrosmo.unam.mx (YG)

suggest the existence of a binary central star. The main shell presents a bipolar morphology consisting of a bright equatorial toroid and two faint bipolar lobes (Aaquist & Kwok 1990; Kwok & Aaquist 1993, hereafter KA93; Miranda 1995, hereafter M95). An external ring-like structure, characterized by relatively high [N II]/Hα values, surrounds the bright toroid (M95). Two highly collimated, high-velocity bipolar knots have been detected along the main nebular axis (PA $\simeq$ 320°) via high-resolution, long-slit spectroscopy (M95). These knots present the typical properties of collimated outflows in PNe (e.g. Miranda 1999), although they also exhibit large differences in radial velocity and velocity width. Another collimated structure was also identified near the major nebular axis (M95). It shares some properties with the bipolar knots (small velocity dispersion, small size, strong [N II] emission), but it does not share the general inclination of the bipolar shell and the bipolar knots. On the basis of these observations, it has been suggested that a mass-transferring binary central star could be involved in the formation of Hu 2-1 (M95). There are additional structural components in this complex PN. The 3.6-cm continuum map by KA93 reveals a small elliptical structure embedded in the toroid, suggesting that Hu 2-1 is a double-shell PN, and a faint extended halo has been detected in long-slit spectra (M95). Moreover, irregular variations of 0.2–0.3 mag in *UBV* have been reported (Kostyakova 1992; Arkhipova et al. 1994). Acker et al. (1998) analysed *Hipparcos* data and measured a proper motion for Hu 2-1 of $\simeq 15 \times 10^{-3}$ arcsec yr^{-1} towards PA $\simeq$ 157°. In addition, Acker et al. obtained a very small, unrealistic distance for Hu 2-1, which, according to the authors, could be due to influence of the nebula itself on the parallax measurement. We will therefore adopt here a distance of 2.35 kpc (see M95).

We have obtained different data on Hu 2-1 in order to study in more detail the different nebular components, testing the binary scenario. In this paper we present the results obtained.

2 OBSERVATIONS AND RESULTS

2.1 Optical imaging

Direct images of Hu 2-1 were obtained with the 2.56-m Nordic Optical Telescope (NOT)[1] at Roque de los Muchachos Observatory in 1996 August. The detector was a Tektronix 24-μm CCD with 1024 × 1024 pixels. The scale in the focal plane is $\simeq$0.176 arcsec pixel^{-1}. The filters were: Hα ($\lambda_0 \simeq 6563$ Å, FWHM $\simeq$9 Å), [N II] ($\lambda_0 \simeq 6584$ Å, FWHM $\simeq$9 Å) and [O III] ($\lambda_0 \simeq$ 5007 Å, FWHM $\simeq$30 Å). Exposure times were 20 s in Hα, 180 s in [N II] and 60 s in [O III]. The seeing was $\simeq$0.72 arcsec for the three images.

Fig. 1 presents contour plots of the Hα, [O III] and [N II] images deduced from the ground-based data. Although the resolution of the ground-based images is lower than those of the *HST* (described below), we present the ground-based images because they are useful to compare with the long-slit spectra (Section 2.3) and to obtain a global view of the excitation conditions in the nebula (see below). By comparing the images with the spectra previously presented (M95), the different structures can be identified. These are labelled in the [N II] image. Structure A corresponds to the bright equatorial toroid. It appears elongated along the nebular minor axis (PA 50°) in Hα and [N II], but circular in [O III]. The bipolar lobes correspond to structure B. C1–C2 are the compact knots along the nebular major axis. C3–C4 are two compact structures at PA $\simeq$ 350°, reported for the first time in this paper. Component D is revealed to be an elongated structure oriented almost perpendicular to the nebular major axis. The images confirm that no counterpart of D exists towards the NW (M95). The existence of the extended (size $\simeq$ 14 arcsec) halo is confirmed. Structures within the halo can be recognized near the north–south direction, almost coinciding with C3–C4, and along PA $\simeq$ 80°. In addition, a bright region within the halo is observed along the nebular minor axis up to $\simeq$6 arcsec from the centre.

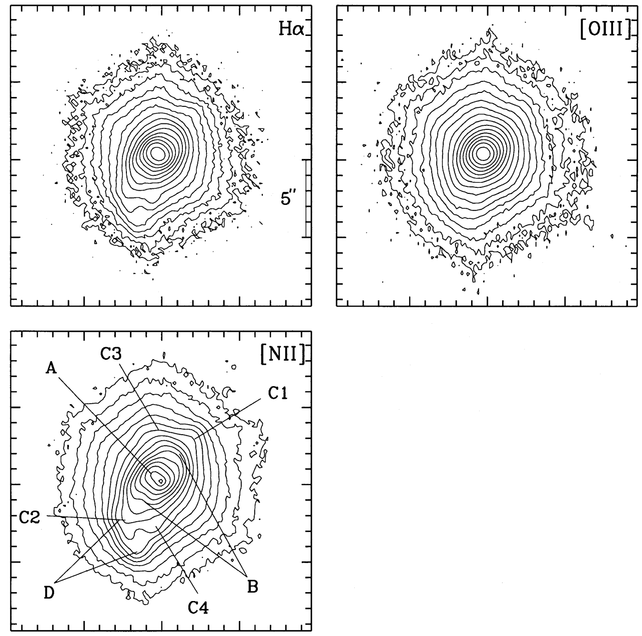

Figure 1. Hα, [O III]5007 and [N II]6583 contour maps of Hu 2-1 from the ground-based images. North is up, and east to the left. The contours are logarithmic separated by a factor of 1.78 in intensity, and have been chosen in order to show up the main features of the nebula. The identified morphological components are indicated in the [N II] image (see text).

In order to gain a better view of Hu 2-1, we have retrieved the WFPC2 Hα, [N II] and PC [O III] images obtained with the *Hubble Space Telescope* from the *HST* archive (program ID: 6347, PI: K. J. Borkowski and J. P. Harrington for the Hα and [N II] images; program ID: 3603, PI: M. Bobrowski for the [O III] image). Fig. 2 shows grey-scale maps of the [N II] image, and Fig. 3 presents a grey-scale map of the central nebular regions as deduced from the Hα image. The *HST* images confirm the basic bipolar structure of the nebula deduced from long-slit observations (M95). The bright toroid resembles a cylinder. If we assume a circular cross-section, the axis of the toroid is tilted $\simeq$37° with respect to the plane of the sky, in excellent agreement with the inclination angle deduced from long-slit spectra (M95). A small structure within the toroid is also observed and corresponds to the inner elliptical shell identified by KA93. This inner shell is extremely faint in [N II] but very bright in Hα and [O III] (not shown here). The *HST* images show that this shell presents open ends (see also below). The bipolar lobes also present point-symmetry with respect to the central star, but they are not symmetric with respect to the main nebular axis. In particular, if we consider PAs 310° and 330°, which are symmetric with respect to the main axis (PA 320°), the lobes are more extended at PA

[1] The Nordic Optical Telescope is operated on the Island of La Palma by NOTSA in the Spanish Observatorio del Roque de los Muchachos of the Instituto de Astrofísica de Canarias.

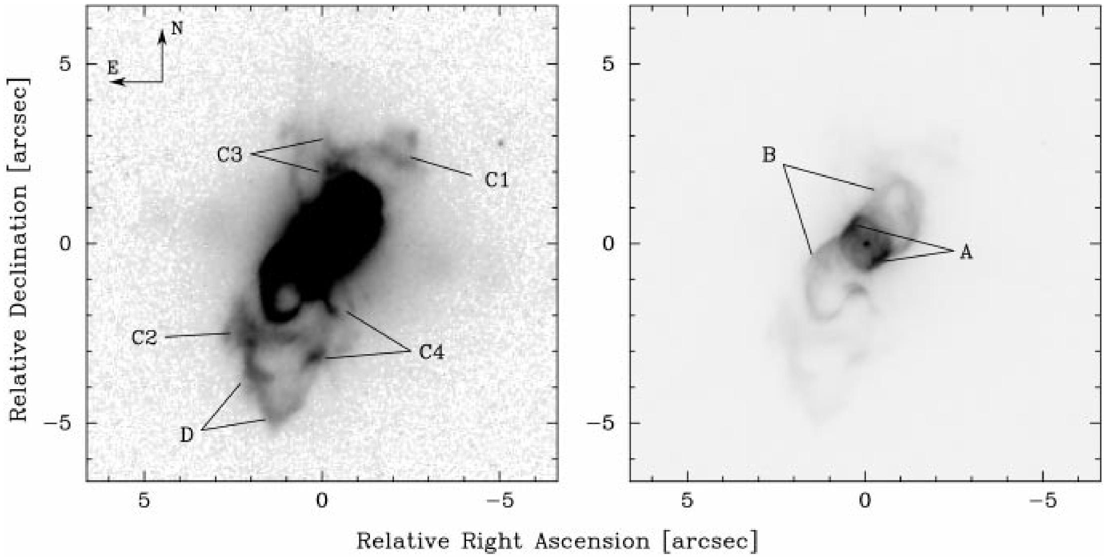

Figure 2. *HST* image of Hu 2-1 obtained in the [N II]6583 line. Two different grey levels have been chosen in order to show both faint and bright nebular structures. The morphological components are indicated (see also Fig. 1).

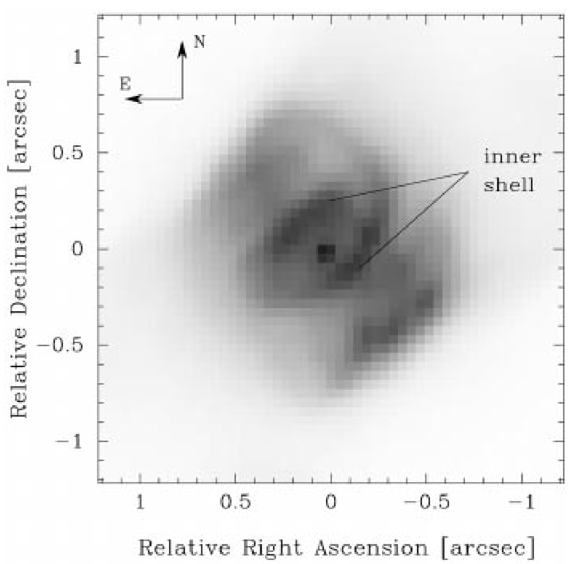

Figure 3. Grey-scale map of the central regions of Hu 2-1 as observed in the Hα line with the *HST*. The inner shell is indicated.

330°, radius $\simeq$2.2 arcsec, than at PA 310°, radius $\simeq$ 1.9 arcsec. Finally, an elongated faint structure, particularly bright in Hα, is observed at PA $\simeq$ 80°, and corresponds to that identified in the ground-based images.

The central star is clearly observed in the *HST* images (Figs 2 and 3). As a remarkable result, we find that its position does not coincide with the centre of the toroid, but it is slightly displaced towards the SW along the nebular minor axis. A displacement of $\simeq$0.05 arcsec (120 au) is obtained from the [N II] and Hα images with respect to the centre of the toroid, and from the Hα and [O III] images with respect to the centre of the inner shell.

The high resolution of the *HST* images allows us to study the structure of C1–C4 and D in detail. C1 and C3 consist each of two small and close knots. In the case of C1, the long-slit spectra (M95; see his fig.4) show two knots at different radial velocity and separated by $\simeq$0.9 arcsec, in agreement with the *HST* [N II] image. In C2 no evidences for more than a knot are found, taking into account that part of the emission near the position of C2 corresponds to structure D (see M95). In the case of C4, a bright knot can be distinguished near the SE lobe and a fainter one at $\simeq$4 arcsec from the centre, which could be related to structure D. D appears as several bow-shock-like structures at different orientations.

Fig. 4 presents image ratios deduced from the ground-based images, which have been used to study the global variations of the excitation conditions in Hu 2-1. A wealth of structure is observed in these images. The innermost nebular regions are of relatively high excitation, whereas the edges of the bipolar lobes and the toroid present a relatively low excitation. Point-symmetry in the lobes can also be recognized in the excitation conditions. Low excitation is observed in C1 to C4 and D. The variation of the excitation along the nebular minor axis is particularly interesting. Close to the edges of the toroid (along PA 50°), we observe a relatively low-excitation zone. The excitation increases outwards, and two high-excitation maxima are observed at $\simeq$2.5 arcsec from the centre. These maxima are very prominent in [O III]/[N II], and seem to form part of a distinct high-excitation circular region which is better observed in [O III]/Hα. Beyond this high-excitation region, Hα dominates in a band along the equatorial plane up to $\simeq$6 arcsec from the centre. The ratio maps also show a region dominated by Hα at PA $\simeq$ 80° up to $\simeq$4 arcsec from the centre (see above).

2.2 Radio observations

The observations were carried out with the Very Large Array (VLA) of the National Radio Astronomy Observatory (NRAO)[2] during 1995 July with the VLA in its A configuration. The data were obtained in the spectral line mode in order to study the H92α recombination line [$\nu = 8309.383$ MHz (3.6 cm)]. We used a bandwidth of 6.25 MHz with two circular polarizations centred at the LSR velocity of 33.3 km s^{-1} and 63 channels of 97.7 kHz

[2] The NRAO is a facility of the National Science Foundation, operated under a cooperative agreement with Associated Universities, Inc.

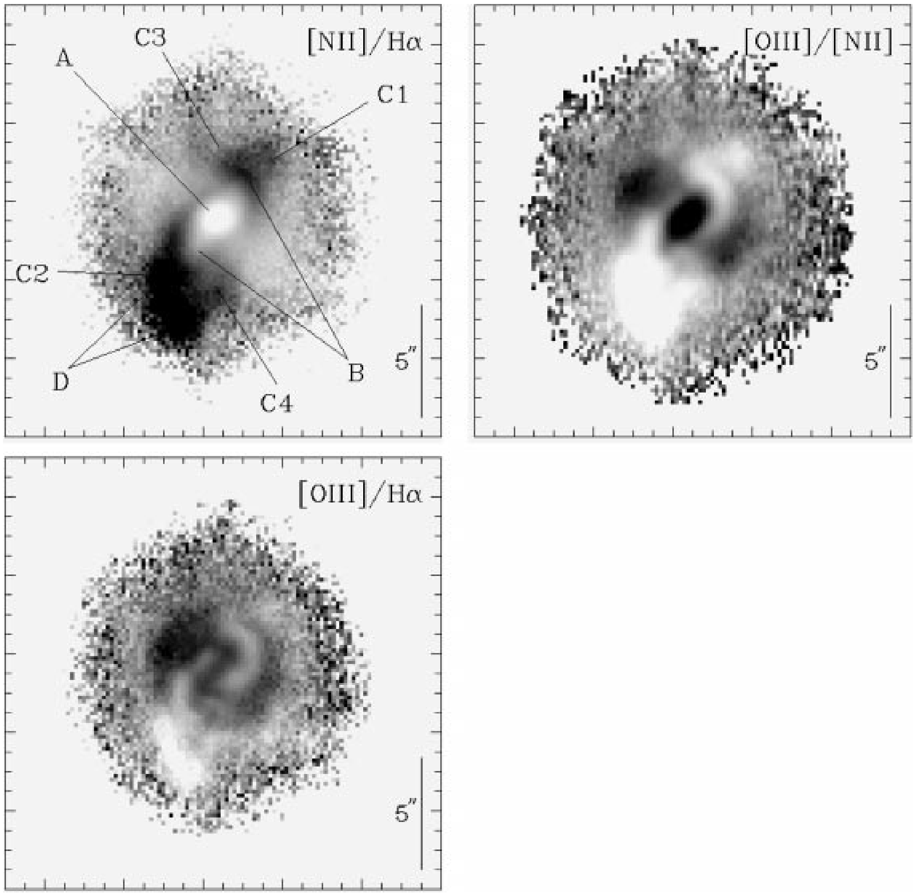

Figure 4. Grey-scale ratio maps of Hu 2-1 obtained from the images in Fig.1. North is up, a east to the left. In each image ratio, black regions refer to high ratios, white regions refer to low ratios.

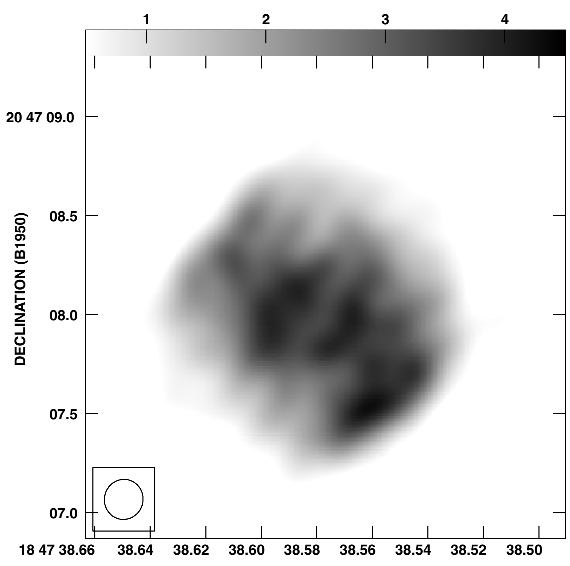

Figure 5. Grey-scale representation of the 3.6-cm continuum map with uniform weighting (beam 0.20×0.19 arcsec^2, PA $- 14°$). The grey-scale levels (top scale) are in mJy beam^{-1}.

($\simeq$3.5 km s^{-1}) wide each, plus a continuum channel (channel 0) which contains the central 75 per cent of the total bandwidth. Integration time was $\simeq$2.5 h, with $\simeq$20 per cent of this time spent in calibration. 3C 286 and 1923+210 were used as flux and phase calibrators, respectively. Calibration and image processing were carried out with the Astronomical Image Processing System (AIPS) of the NRAO. Continuum emission at 3.6 cm and H92α emission were detected from Hu 2-1. We show in Fig. 5 a grey-scale map of the 3.6-cm continuum emission obtained with uniform weighting of the (u,v) data (beam $= 0.20 \times 0.19$ arcsec, PA $= -14°$). In Fig. 6 we show contours of the H92α emission obtained by adding all channels in which line emission is detected (from 19 to 51 km s^{-1}), superposed on a 3.6-cm continuum map made with natural weighting and a Gaussian taper of 500 kλ (beam $= 0.42 \times 0.40$ arcsec^2, PA $= 60°$). The continuum flux density at 3.6 cm is $\simeq$110 mJy, compatible with the value obtained by KA93. The H92α flux density is $\simeq$3.9 mJy.

The 3.6-cm continuum map (Fig. 5) shows the innermost regions of Hu 2-1 in considerable detail. The bright regions separated $\simeq$1 arcsec at PA $\simeq$ 50° correspond to the outer edges of the toroid. The inner shell, identified by KA93, can be distinguished with a size of $\simeq$0.35 arcsec and with the major axis near PA 320°. In our map, it shows open ends and a clear point-symmetric brightness distribution. Detection of H92α emission is restricted to a region of $\simeq$0.5 arcsec in radius, apparently coinciding with the inner shell (Fig. 6). We note that given the intensity of the continuum emission in the outer edges of the toroid, one would expect to detect H92α emission from these positions as well. However, the continuum emission towards the edges of the toroid is probably optically thick, preventing the detection of H92α emission.

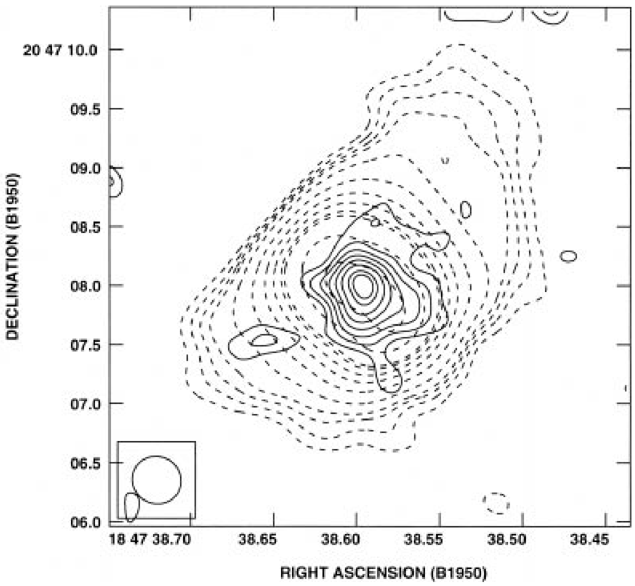

Figure 6. Contour map of the velocity-integrated H92α emission (solid line) superposed on a contour map of the 3.6-cm radio continuum emission (dashed line) made with natural weighting and a Gaussian taper of 500 kλ, which resulted in a synthesized beam of 0.42×0.40, PA 60°. The levels for H92α are 30, 40, 50, 60, 70, 80, 90 and 95 per cent of the maximum of 50.2 mJy beam^{-1} km s^{-1}. Radio continuum contour levels are 3, 5, 7, 9, 15, 30, 50, 70, 90, 100, 150 and $200 \times 7.1 \times 10^{-2}$ mJy beam^{-1}, the rms noise of the map. The peak position of the radio continuum map is $\alpha(1950) = 18^{h}47^{m}38^{s}.60$ and $\delta(1950) = 20°47'08''.0$.

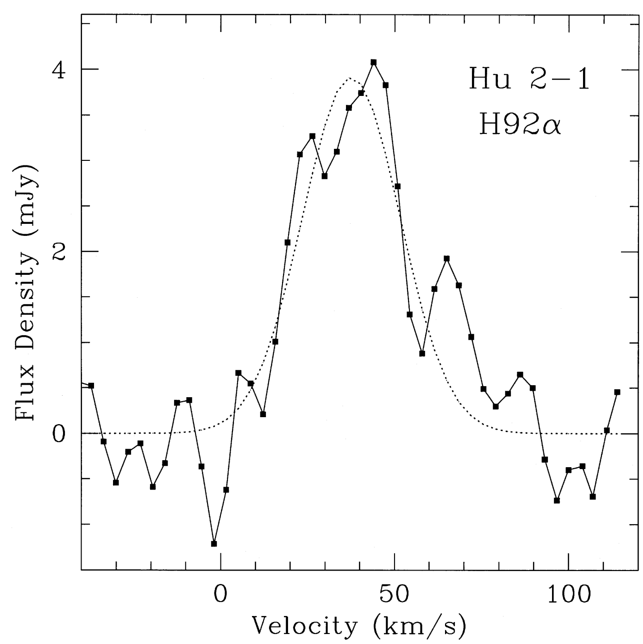

Figure 7. H92α emission profile. The dotted line shows a Gaussian fit to the line profile.

Fig. 7 presents the H92α line profile. The LSR central velocity and the linewidth (FWHM) of the H92α emission have been determined by means of a single-Gaussian fit, and are listed in Table 1. Given the reduced S/N of the profile, the deduced systemic velocity ($V_{\mathrm{LSR}} \simeq 37 \pm 2$ km s^{-1}) is compatible with that deduced from optical emission lines (see below). Because of the low S/N in the individual channels, a detailed study of the kinematics in H92α is not possible. In order to increase the S/N, we have added the blueshifted channels and the redshifted channels with respect to the systemic velocity as deduced from the optical lines. The result is presented in Fig. 8. Blueshifted emission appears slightly displaced towards the NNW, with respect to the emission centre in the continuum image, whereas redshifted emission is displaced towards the SSE.

Table 1. Physical parameters of Hu 2-1[a].

Parameter	Value
S_ν(continuum) (mJy)[b]	110 ± 1
S_ν(line) (mJy)[b]	3.9 ± 0.3
V_{LSR} (km s^{-1})[c]	37 ± 2
ΔV_{L} (km s^{-1})[c]	33 ± 2
T_{e} (K)[d]	7000 ± 500
N_{e} (cm^{-3})[e]	5900 ± 100

[a] Obtained from continuum and H92α observations at 3.6 cm, following the formulation by Mezger & Henderson (1967).
[b] Total continuum and integrated line flux density.
[c] Systemic velocity and velocity width of the H92α line, determined by a Gaussian fit.
[d] Electron temperature, assuming a distance of 2.35 kpc (see text).
[e] Electron density.

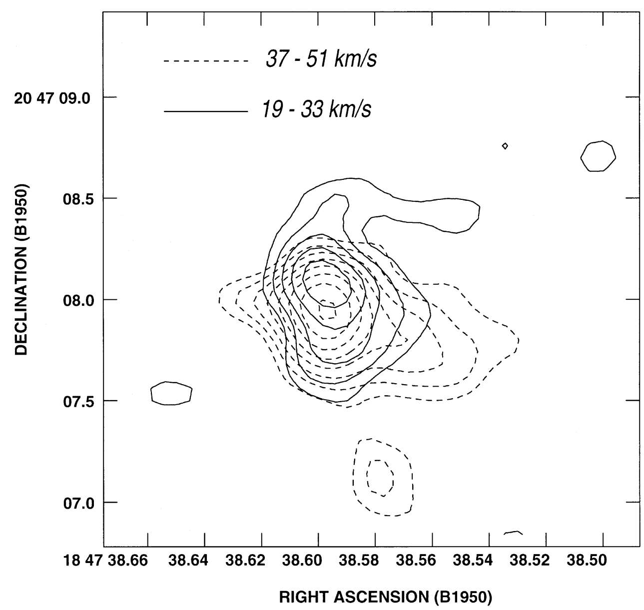

Figure 8. Contour maps of the H92α emission for the two velocity intervals indicated at the top. Solid contours represent blueshifted emission, and dashed contours represent redshifted emission with respect to the systemic velocity.

Estimates for the electron density and electron temperature were obtained from the continuum and line emission following the formulation by Mezger & Henderson (1967), assuming that the gas is in LTE and from the observed line-to-continuum ratio $T_{\mathrm{C}}/T_{\mathrm{L}}$ of $\sim$12.5. The results are listed in Table 1. The values obtained for the electron density and temperature are similar to

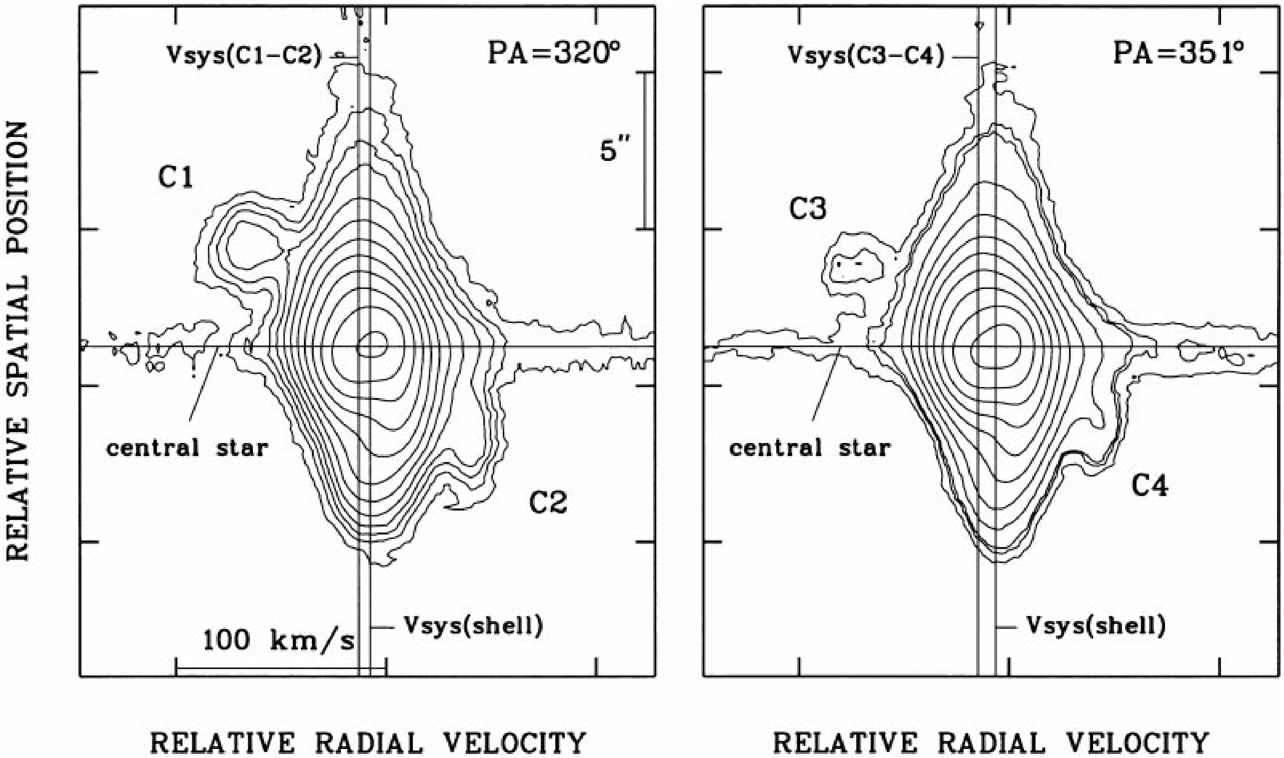

Figure 9. Position–velocity contour maps of the [N II]6583 long-slit spectra. The position angle of the slit is indicated in the upper right corner. The contour are logarithmically separated by a factor of 2 in intensity. The knots C1, C2, C3 and C4 are indicated. The position of the central star is represented by the position of the intensity maximum of the continuum. V_{sys}(shell) indicates the systemic velocity of the main nebular shell, whereas V_{sys}(C1–C2) and V_{sys}(C3–C4) indicate the systemic velocity of the two pairs of compact knots (see text for details).

those obtained from optical emission lines (see M95, and references therein).

2.3 Long-slit spectroscopy

Long-slit spectra were obtained in 1998 August with IACUB[3] at the NOT. A filter was used to isolate the Hα and [N II]6583 emission lines. Two spectra were obtained at PAs 320° and 351° with the slit centred on the object. The exposure time was 900 s for each spectrum. A Th-Ar lamp was used for wavelength calibration. The spectral resolution (FWHM) is $\simeq 8\,\mathrm{km\,s^{-1}}$. Seeing was $\simeq$1.4 arcsec. The data were reduced using standard procedures within the IRAF[4] and MIDAS packages. The error in absolute radial velocity is estimated to be $\simeq \pm 1.2\,\mathrm{km\,s^{-1}}$. However, the internal accuracy in each long-slit spectrum is much better, $\simeq \pm 0.15\,\mathrm{km\,s^{-1}}$. Contour plots of the [N II]6583 emission line, in a position–velocity representation, are shown in Fig. 9. As compared with the spectra presented by M95, the new ones, though with poorer spatial resolution, have a higher spectral resolution and provide information about the bipolar knots C3–C4.

Table 2 lists different parameters of the knots C1 to C4 (PA, radial velocity, angular position and spectral and angular widths) obtained from the spectra. Radial velocities and angular positions refer to the centroid of the knots. The radial velocities are quoted with respect to the systemic velocity of the main nebular shell [V_{sys}(shell)] (hereafter considered as the toroid and bipolar lobes) for which we deduce $V_{LSR} = 34.5 \pm 1.2\,\mathrm{km\,s^{-1}}$ ($V_{\odot} = 15.1\,\mathrm{km\,s^{-1}}$) in agreement with previous determinations (Schneider et al. 1983; M95; Durand, Acker & Zijlstra 1998). Spatial positions have been determined with respect to the central star, represented by the position of the maximum of the stellar continuum in the two-dimensional frames, with a precision of $\simeq \pm 0.1$ arcsec. The results for C1–C2 are compatible with those obtained by M95, the small differences being due to the fact that in Table 2 the parameters refer to the centroid of the knots, whereas M95 considered the peak intensity. In addition, the new spectra show that C3–C4 constitutes a system of highly collimated bipolar knots.

The following results are noticed from Table 2. The radial velocity of the NW knots C1 and C3 is systematically higher than that of their corresponding SE counterparts C2 and C4. In particular, the radial velocity of C1 is $11\,\mathrm{km\,s^{-1}}$ higher than that of C2, and the radial velocity of C3 is $16\,\mathrm{km\,s^{-1}}$ higher than that of C4. The radial velocity decreases with the distance in C1 and C3. In fact, the position–velocity maps (Fig. 8) suggest that two knots at different velocities are present in C3. Within C2 and C4 the radial velocity is constant (see also M95). C1–C2 are located at greater distance from the central star than C3–C4. However, differences in the distance for the knots in a particular pair do not seem to be significant. C1 and C3 present a higher velocity width than C2 and C4. This can be explained taking into account the fact that C1 and C3 consist of two small knots at different velocity (see above), and therefore the velocity width results from the

[3] The IACUB uncrossed echelle spectrograph was built in a collaboration between the IAC and the Queen's University of Belfast.

[4] IRAF is distributed by the National Optical Astronomy Observatory, operated by the Association of Universities for Research in Astronomy, Inc. (AURA) under cooperative agreement with the National Science Foundation.

Table 2. Parameters of the knots C1, C2, C3 and C4[a].

Knot	PA (degrees)	$V_r{}^b$ (km s^{-1})	X^c (arcsec)	ΔV^d (km s^{-1})	ΔX^e (arcsec)
C1	320	−59	3.0	28	1.4
C2	140	+48	3.0	17	1.5
C3	351	−66	2.5	29	1.3
C4	171	+50	2.4	19	1.6

[a] Obtained from the long-slit [N II] spectra shown in Fig. 9.
[b] Radial velocity with respect to the systemic velocity of the main nebular shell ($V_{LSR} = 34.5$ km s^{-1}).
[c] Angular distance from the central star along the corresponding PA.
[d] Velocity width (FWHM) corrected of spectral resolution.
[e] Spatial extent (FWHM) corrected of spatial resolution.

superposition of two knots which are not spatially resolved in our spectra.

The results for the toroid and bipolar lobes are compatible with those obtained by M95. In the case of D, we confirm the previous results – in particular, its very low radial velocity (between −2 and +2 km s^{-1}; see M95 for details).

3 DISCUSSION

In the following we will discuss possible interpretations for the data presented above, testing the scenario of a binary system at the centre of Hu 2-1.

3.1 Shaping of the inner and bipolar shells

The data suggest that the inner shell could be (1) an elliptical, independent shell (see KA93), (2) the inner 'walls' of the toroid, or (3) a second, inner toroid concentric with the outer one. The kinematics of this shell can be used to decide between these possible interpretations. As already mentioned, the H92α emission seems to be related to the inner shell. If this shell represents the inner walls of the toroid or a second toroid concentric with the outer one, it would be expected to detect the H92α emission blueshifted (redshifted) towards the SE (NW) part of the toroid, according to its inclination (M95). However, the opposite is found (Section 2.2, Fig. 8), as would be expected if the H92α emission traces an expanding ellipsoidal shell with the NW (SE) part blueshifted (redshifted) as the bipolar lobes or a toroid with a different inclination from the outer one. Nevertheless, these interpretations do not explain the point-symmetry of the inner shell, which suggests the existence of a non-spherical wind interior to the inner shell, at scales $\leq$0.35 arcsec, which is not oriented along the major nebular axis and impacts the inner shell at certain angle. It is possible that the H92α emission could be tracing a bipolar outflow interior to the inner shell. The foreseen upgrading of the VLA will certainly allow us to study with great sensitivity and high resolution the innermost regions of the nebula.

With regard to the bipolar shell, the equatorial toroid expands at $\simeq$15 km s^{-1} in [N II] (M95), and the *HST* [N II] image indicates a size of $\simeq$1.1 arcsec, so that its kinematic age is $\simeq$410 yr. The bipolar lobes expand at $\simeq$30 km s^{-1} (M95), and the *HST* images indicate a maximum radius of $\simeq$2.2 arcsec at PA 330°. The bipolar axis is tilted $\simeq$37° with respect to the plane of the sky. With these numbers, the kinematic age of the bipolar lobes would be $\simeq$1000 yr, much larger than the age of the toroid. This difference can be explained if the kinematics of the lobes is more complex than previously assumed (M95). In fact, the maximum size of the lobes is observed along PA 330° where the largest departures from axial symmetry are observed. It is plausible that these regions are expanding at a higher velocity than $\simeq$30 km s^{-1}, and/or are tilted at an angle different from 37°. Therefore the kinematic age of the toroid probably is more representative for the age of the bipolar shell.

In any case, the shape of the bipolar lobes points out to a bipolar wind interior to the main shell. In an idealized model of interacting stellar winds (see Zhang & Kwok 1998, and references therein), the lobes in a bipolar PN should be symmetric with respect to the bipolar axis. This is not the case for the lobes in Hu 2-1, which show clear departures from axis-symmetry. As in the case of the inner shell, we propose the existence of an interior bipolar wind which is not oriented along the main nebular axis, but impacts the lobes at certain angle, so that the lobes are inflated in an asymmetric (with respect to the main nebular axis) but point-symmetric (with respect to the central star) manner. Interaction of collimated outflows with shells has been suggested to occur in other PNe (Sahai & Trauger 1998; Miranda et al. 1999; Vázquez et al. 1999, 2000). We note that in the case of Hu 2-1, however, knots C1 to C4 do not seem to be involved in shaping the bipolar lobes, because evidence for interaction between the knots and lobes cannot be recognized in our data. If interaction had existed, one would expect strong deformations of the lobes at the PAs where the knots are detected (see, e.g., Miranda et al. 1999), which is not observed. The origin of the interior bipolar wind is difficult to elucidate from the observed geometry alone. It could be either that the fast stellar wind from the central star is anisotropic in origin, or that two winds are present: an isotropic fast stellar wind from the central star, and an intrinsically bipolar wind from a companion.

3.2 The structure of the equatorial plane

The image ratio maps show an equatorial zone within the halo, which is characterized by peculiar line ratios, particularly those involving Hα. This suggests the existence of a flat equatorial region with physical conditions different from those in other parts of halo. A plausible interpretation for this equatorial region is that it is related to, and traces anisotropic mass ejection during the AGB phase of the Hu 2-1 progenitor. In fact, for an expansion velocity of 10 km s^{-1}, the kinematic age of the flat region is $\simeq$7000 yr, much greater than that of the main shell. Taking into account the fact that the transition time from AGB to PN is $\simeq$2000–3000 yr and the evolutionary time in the AGB is $\simeq 10^6$ yr, the formation of this region has occurred in the very late stages of AGB evolution. The distinct high-excitation region within the halo is younger, $\simeq$2800 yr, also assuming a velocity of 10 km s^{-1}. This region could represent the final ejection in the AGB before the object entered in its proto-PN phase. The high excitation in this region could be related to hardening of the radiation as observed in high-excitation haloes of PNe (Guerrero & Manchado 1999).

Different mechanisms have been suggested to produce anisotropic mass-loss during the AGB, including stellar rotation, magnetic fields, non-radial pulsations, and binarity (Soker 1996, and references therein; García-Segura et al. 1999; Mastrodemos & Morris 1999). In many cases, the presence of a companion is required either to spin up the envelope of the AGB star or to deflect the mass towards the equatorial plane (see, e.g., Soker 1996). However, García-Segura et al. (1999) have recently modelled single stars rotating at near-critical rotation rates at the end of the AGB stage. These models also produce ejection towards the equatorial plane and, when combined with an interacting winds scenario and magnetic fields, they are capable to account for the large variety of shapes observed in PNe (García-Segura et al. 1999). In the case of Hu 2-1, the simple detection of an equatorial ring-like structure ejected during the end of the AGB stage does not allow us to discriminate between single-star or binary scenarios.

3.3 The off-centre position of the central star

Off-centre central stars are observed in many PNe (see Soker 1999, and references therein). We compare Hu 2-1 with MyCn 18 (Sahai et al. 1999), which are considered to be at a similar distance. In both cases, the central star is displaced along the nebular minor axis. In Hu 2-1, the displacement is $\simeq$120 au, while larger displacements, between 270 and 1150 au, are found in MyCn 18 with respect to different nebular structures (Sahai et al. 1999). A possibility to explain a displaced central star is relative proper motion of the central star and nebula. In Hu 2-1 this possibility can be ruled out, because the proper motion vector of the nebula is perpendicular to the direction of displacement (Acker et al. 1998). Another possibility to be considered is binarity of the central star. Soker (1994) and Soker, Rappaport & Harpaz (1998) model the influence in the nebular morphology of wide and eccentric close binaries, respectively. In both cases, off-centre central stars are predicted. Hu 2-1 fits much better the eccentric scenario because (1) the displacement is observed along the minor nebular axis, and (2) bipolar PNe could be related to eccentric binaries (see Soker et al. 1998). According to these authors, orbital separations of 7–80 au and orbital periods of 15–500 yr are suggested for this kind of eccentric close binaries (see Section 3.5).

3.4 Collimated outflows and possible detection of orbital motion

The new data have revealed the existence of multiple collimated knots in Hu 2-1 at different directions. Whereas C1–C2 and C3–C4 represent the typical bipolar collimated outflows observed in PNe, the nature of D is less clear. The bow-shock appearance suggests that D could represent a series of collimated outflows. In this case, the outflows should have been monopolar, and either they move almost perpendicular to the line of sight or their expansion velocity is very low. In any case, D does not share the general inclination of the nebula. We note that D is located towards the SE, coinciding with the direction of the proper motion of Hu 2-1 (Acker et al. 1998). Therefore it is possible that the formation of D could be related to interaction of the nebula with the interstellar medium.

The properties of the collimated outflows C1–C2 and C3–C4 suggest a precessing ejection source. These kind of outflows is much better accommodated by a binary scenario than into a single-star one (see below). Single-star models have been able to explain jets in PNe if stellar rotation and magnetic fields are considered (García-Segura et al. 1999). This model produces jets along the main nebular axis. If precessing jets are to be explained within these models, a companion to the central star is required (García-Segura 1997). Therefore the mere presence of collimated outflows at different directions in Hu 2-1 suggests a binary central star.

The most striking result concerning the bipolar outflows is the systematic difference between the radial velocities of the two knots in each bipolar pair. This could be attributed to differences in the ejection velocity (M95). In this case, systematic differences in position of the knots with respect to the central star would be expected, but they are not observed. Another possibility is deceleration of the knots by interaction with nebular material. If so, deceleration should have been more conspicuous in C2 and C4, the knots with lower radial velocity. However, evidence for deceleration exists in C1 and C3, which show an internal decrease of the radial velocity (see Section 2.3), but not in C2 and C4 in which the radial velocity is constant. We also note that a combination of different ejection velocity, different ejection angle and selective deceleration is highly improbable because of the very peculiar combination of these parameters necessary to explain the systematic differences in radial velocity and the symmetric location of the knots in each pair with respect to the central star.

In order to explain these results, we consider a completely different and novel point of view, namely, that the differences in radial velocity arise only because we have measured them with respect to V_{sys}(shell) which, in this case, is a misleading reference system for the collimated outflows. In other words, we suggest that the systemic velocity of the main nebular shell does not coincide with the systemic velocity of the collimated knots. Remarkably, this situation is what one would expect from a binary ejection source. The systemic velocity of the main nebula is related to material ejected during the last stages of the AGB phase averaged over a relatively large time-span and over many orbits. In a first approximation, the average velocity of the ejection will be the same in all directions, and the systemic velocity will not contain information about the orbital velocity or about a particular orbital position (but see below). The collimated knots, however, can be considered as 'instantaneous' ejections, given their compactness. Their space velocities will contain two components: the component due to the own ejection velocity, and the component due to the 'instantaneous' orbital velocity at the time of ejection. The component due to the orbital velocity will be added with the same sign to the component due to its own ejection velocity in each knot of a bipolar pair. As a consequence of the additional orbital component of the velocity, the systemic velocity of the knots will be shifted with respect to V_{sys}(shell).

The data in Table 2 allow us to obtain the systemic velocity and the radial velocities of the knots with respect to their own systemic velocity. For C1–C2 we obtain $V_{\mathrm{sys}}(\mathrm{C1–C2}) = 29\,\mathrm{km\,s^{-1}}$ and a radial velocity of $\pm 53.5\,\mathrm{km\,s^{-1}}$ with respect to V_{sys}(C1–C2). For C3–C4, V_{sys}(C3–C4) is $26.5\,\mathrm{km\,s^{-1}}$ and the radial velocity is $\pm 58\,\mathrm{km\,s^{-1}}$ with respect to V_{sys}(C3–C4). The three systemic velocities V_{sys}(C1–C2), V_{sys}(C3–C4) and V_{sys}(shell) are represented in Fig.9. Both V_{sys}(C1–C2) and V_{sys}(C3–C4) are blue-shifted with respect to V_{sys}(shell) by 5.5 and $8\,\mathrm{km\,s^{-1}}$, respectively. These values are noticeable larger than the relative errors (Section 2). In addition, V_{sys}(C1–C2) and V_{sys}(C3–C4) are almost identical to each other within the absolute errors. In the following, we will consider as radial velocity of the knots that referred to their own systemic velocity.

Estimates for the expansion velocity, distance to the central star and kinematic age of the collimated outflows can be obtained if the inclination angle is known. The location of C1–C2 along the major nebular axis suggests that C1–C2 move along that axis

(M95). However, this is not necessarily true. For instance, some parts of D also project along the major axis, but they move in a completely different direction. In addition, we note that for inclinations of C1–C2 $\leq 40°$, the kinematic age of the knots is lower than that of the toroid. This would imply interaction of the collimated knots with the shell, which is not observed (see above). Therefore we will assume a range of 40°–60° for the inclination of C1–C2, and a constant velocity for the two pairs. We obtain a range of outflow velocities between 60–85 km s^{-1}, and a range of kinematic ages for C1–C2 between 520–1100 yr. The difference of kinematic ages between C1–C2 and C3–C4 is $\simeq$ 15–100 yr.

3.5 Binary parameters and implications for jet formation in Hu 2-1

The available information can be used to constrain the characteristics of the binary central star in Hu 2-1. From the simple model outlined above (Section 3.4), it can be easily demonstrated that

$$V_{\rm sys}(\text{knots}) - V_{\rm sys}(\text{shell}) = V_{\rm orb} \times \cos(\gamma) \times \cos(i), \tag{1}$$

where $V_{\rm orb}$ is the orbital velocity at the time of ejection, γ is the angle between the orbital velocity vector and the line of sight, and i is the inclination angle of the orbital plane with respect to the line of sight. For $V_{\rm sys}$(knots) – $V_{\rm sys}$(shell) we obtain 5.5–8 km s^{-1}. In addition, it is reasonable to assume that the orbital plane coincides with the equatorial plane of the nebula, which is tilted $\simeq$37°. With these assumptions, we obtain $V_{\rm orb} \times \cos(\gamma) \simeq$ 10 km s^{-1}, which is a lower limit to the orbital velocity. For masses $M_1 + M_2$ in the range 1–3 M$_\odot$, we obtain upper limits for the orbital separation of $\simeq$ 9–27 au (assuming circular orbit; see also below) and for the period of $\simeq$25–80 yr. It is worth noting that these orbital parameters are in the range of those expected from the displacement of the central star (Section 2.1). Therefore the true orbital separation and period should not be much lower than the obtained upper limits, which also implies that the orbital velocity should not be much larger that the deduced value.

Two basic binary scenarios have been suggested to explain the generation of precessing collimated outflows in PNe. A scenario is that of a mass-transferring binary (Morris 1987; Soker & Livio 1994; Mastrodemos & Morris 1998). In this scenario, mass lost from the AGB star is partially captured by the secondary forming an accretion disc around it, from which collimated outflows are produced. Precession of the accretion disc will result in changes of the direction of the collimated outflows. A different scenario is considered by Soker & Livio (1994) and Soker (1996), in which a disc is formed around the AGB nucleus by Roche lobe overflow and destruction of a stellar or substellar companion. In this case, the jets emanate from the AGB star. Radiation may induce self-warping of the disc, so that the disc precesses originating precessing outflows (Livio & Pringle 1996). In the first case, models by Mastrodemos & Morris (1998, 1999) indicate that accretion on to the secondary is effective at large orbital separations ($\simeq$24 au). The second scenario requires orbital separations $\leq$2 R$_\odot$ for the secondary being destroyed (Soker 1996; Reyes-Ruiz & López 1999). The binary parameters deduced for Hu 2-1 clearly favour a mass-transferring binary scenario with the collimated ejection generating from an accretion disc around the secondary. Furthermore, the ejection of material towards the equatorial plane is also compatible with a binary with these characteristics (Mastrodemos & Morris 1999).

In the previous calculations, we have assumed circular orbit. This is not necessarily true. In fact, the off-centre position of the central star points out to an eccentric binary (Section 3.3). In this case, the ejection velocity of the AGB wind may depend on the orbital position (Mastrodemos & Morris 1998; Soker 1998), so that the measured systemic velocity of the nebula will contain some information about the orbital velocity. However, the displacement of the central star in Hu 2-1 is small compared, for instance, with that in MyCn 18. In fact, the displacement amounts $\simeq$5–15 per cent in terms of the size of the outer edges of the toroid and inner shell, respectively, which is smaller than the displacement observed in MyCn 18 ($\simeq$25 per cent). This suggests that the ellipticity is small and/or that there is a small dependence of mass-loss with the orbital position. However, without regard to these considerations, the systemic velocities of the two pairs are very similar to each other. From this result and taking into account that the amplitude of the radial velocity curve could be $\sim$20 km s^{-1} (see above), it can be concluded that collimated ejection occurs at a particular orbital phase and may be a ‘periodic’ phenomenon. This suggests that mass accretion is enhanced at some points of the orbit, e.g., through passage by the periastron so that ‘massive’ collimated outflows in the form of bright knots are generated. This conclusion is supported by the similarity between the difference of kinematic ages of the two collimated pairs (15–100 yr) and the orbital period (25–80 yr). At different orbital positions, after ‘massive’ collimated ejection occurs, the bipolar outflow could still be active but with different properties (e.g., mass-loss, velocity, direction, collimation angle), so that collimated knots are not generated. However, the bipolar outflow may still be capable of shaping the bipolar lobes and the inner shell.

The orbital parameters deduced in Hu 2-1 are remarkably similar to those of symbiotic stars (e.g. Seaquist & Taylor 1990). Some symbiotic stars exhibit bipolar shells, equatorial discs and collimated outflows. In particular, we find remarkable similarities between Hu 2-1, R Aqr and HM Sge. The orbital separations and periods of these symbiotic stars are: 18 au and 44 yr for R Aqr, and 25 au and 90 yr for HM Sge (Hollis, Pedelty & Lyon 1997; Richards et al. 1999). Although these parameters are rough estimates, they compare very well to those of Hu 2-1. Moreover, ‘precessing’ collimated outflows are present in R Aqr and HM Sge, as well as a bipolar shell and an equatorial ring-like structure (see Solf 1984, Solf & Ulrich 1985, Hollis, Wagner & Oliversen 1990 and Corradi et al. 1999). We also note that Solf & Ulrich found in R Aqr a difference of 13 km s^{-1} between the systemic velocity of the two bipolar shells, which was attributed to orbital motion. This suggestion is supported by the velocity semi-amplitude for the Mira in R Aqr (Hollis et al. 1997). The possible evolutionary relationship of symbiotic stars with PNe has already been pointed out (Corradi et al. 1999, and references therein). From the results presented in this paper, we suggest that Hu 2-1 represents the result of the evolution of a symbiotic star similar to R Aqr and HM Sge, after the AGB star has evolved towards a central star of PNe.

4 CONCLUSIONS

We have carried out a multiwavelength observational study of the PN Hu 2-1 based on a set of optical/radio data obtained at high spectral and/or spatial resolution. These data have allowed us to identify many structural components in this complex PN. The main shell of Hu 2-1 is bipolar and consists of a toroid and two point-symmetric lobes which also exhibit noticeable departures from axial symmetry. Inside the toroid, an inner point-symmetric shell is observed. Two bipolar pairs of low-excitation knots are identified at different directions, and correspond to collimated outflows. Several monopolar, low-excitation bow-shocks-like structures are observed on one side of the nebula. We confirm the existence of an extended halo around the main nebula. This halo contains a distinct, extended equatorial disc-like region with peculiar excitation conditions.

The early formation of Hu 2-1 seems to be dominated by mass ejection towards the equatorial plane. This anisotropic mass-loss process, resulting in the formation of a flat region within the halo, appears to have been active from the very late stages of AGB evolution up to the onset of the proto-PN phase. However, during the proto-PN and/or PN phase, variable, 'precessing' bipolar collimated outflows appear as the dominant formation mechanism of the nebula. This kind of outflow can be identified not only as two systems of highly collimated bipolar knots at different orientations, but they could also be recognized in the point-symmetry of the bipolar lobes and inner shell, and in the departure from axial symmetry of the bipolar lobes. We also note that interaction with the interstellar medium could also be involved in the formation of the monopolar structures.

The whole set and the consistency of the different results provide strong support for the conclusion that a binary central star has been involved in the formation of Hu 2-1. First-order estimates for the orbital parameters (separation $\sim$9–27 au, period $\sim$25–80 yr) have been deduced from the observed kinematics and a simple binary model. These parameters suggest that the central star of Hu 2-1 is a mass-transferring binary in which collimated ejections are generated from an accretion disc around a companion. There are many similarities between Hu 2-1 and symbiotic stars as, e.g., R Aqr and HM Sge, which lead us to suggest that Hu 2-1 may be the descendant of this kind of binary star.

We suggest that a precise comparison of the systemic velocity of collimated outflows and main shell in other PNe may be a powerful method to detect the effects of orbital motion in a binary central star, and/or to place strong constraints on the possible nature of the central star and on the scenario for the generation of collimated outflows.

ACKNOWLEDGMENTS

We thank the referee for comments which have been very useful for improving the presentation and interpretation of the data. We are very grateful to E. Alfaro, G. Anglada, A. Claret and E. Pérez for useful comments and discussions. LFM and JMT are supported partially by DGESIC PB98-0670-C02 and Junta de Andalucía (Spain). MAG is supported partially by DGESIC of the Spanish Ministerio de Educación y Cultura. YG acknowledges financial support from DGAPA-UNAM and CONACyT-Mexico. RV acknowledges financial support from CONACyT grant I32815E (Mexico). This work has been supported partially by the Programa de Cooperación Científica con Iberoamérica.

REFERENCES

Aaquist O. B., Kwok S., 1990, A&AS, 84, 229
Acker A., Fresneau A., Pottasch S. R., Jasniewicz G., 1998, A&A, 337, 253
Arkhipova V. P., Kostyakova E. B., Noskova R. I., 1994, Pis'ma Astron. Zh., 20, 122
Bond H. E., 2000, in Kastner J. H., Soker N., Rappaport S., eds, Asymmetrical Planetary Nebulae II, From Origin Microstructure, ASP Conf. Ser., Vol. 199. Astron. Soc. Pac., San Francisco, p. 115
Ciardullo R., Bond H. E., Sipior M. S., Fullton L. K., Zhang C.-Y., Schaefer K. G., 1999, AJ, 118, 488
Corradi R. L. M., Ferrer O. E., Schwarz H. E., Brandi E., García L., 1999, A&A, 348, 978
Durand S., Acker A., Zijlstra A., 1998, A&AS, 132, 13
García-Segura G., 1997, ApJ, 489, L189
García-Segura G., Langer N., Rózyczka M., Franco J., 1999, ApJ, 517, 767
Guerrero M. A., Manchado A., 1999, ApJ, 522, 378
Hollis J. M., Pedelty J. A., Lyon R. G., 1997, ApJ, 482, L85
Hollis J. M., Wagner R. M., Oliversen R. J., 1990, ApJ, 351, L17
Kostyakova E., 1992, Pis'ma Astron. Zh., 18, 802
Kwok S., Aaquist O. B., 1993, PASP, 105, 1456 (KA93)
Livio M., Pringle J. E., 1996, ApJ, 465, L55
Mastrodemos N., Morris M., 1998, ApJ, 497, 303
Mastrodemos N., Morris M., 1999, ApJ, 523, 357
Mezger P. G., Henderson A. P., 1967, ApJ, 147, 490
Miranda L. F., 1995, A&A, 304, 531 (M95)
Miranda L. F., 1999, in Guenther E., Stecklum B., Klose S., eds, Optical and Infrared Spectroscopy of Circle Matter, ASP Conf. Ser., Vol. 188. Astron. Soc. Pac., San Francisco, p. 257
Miranda L. F., Vázquez R., Corradi R. L. M., Guerrero M. A., López J. A., Torrelles J. M., 1999, ApJ, 520, 714
Morris M., 1987, PASP, 99, 115
Reyes-Ruiz M., López J. A., 1999, ApJ, 524, 952
Richards A. M. S., Bode M. F., Eyres S. P. S., Kenny H. T., Davis R. J., Watson S. K., 1999, MNRAS, 305, 380
Sahai R., Trauger J. T., 1998, AJ, 116, 1357
Sahai R. et al., 1999, AJ, 118, 468
Schneider S. E., Terzian Y., Purgathofer A., Perinotto M., 1983, ApJS, 52, 399
Seaquist E. R., Taylor A. R., 1990, ApJ, 349, 313
Solf J., 1984, A&A, 139, 296
Solf J., Ulrich H., 1985, A&A, 148, 274
Soker N., 1994, MNRAS, 270, 774
Soker N., 1996, ApJ, 468, 774
Soker N., 1998, ApJ, 496, 833
Soker N., 1999, AJ, 118, 2424
Soker N., Livio M., 1994, ApJ, 421, 219
Soker N., Rappaport S., Harpaz A., 1998, ApJ, 496, 842
Vázquez R., López J. A., Miranda L. F., Torrelles J. M., Meaburn J., 1999, MNRAS, 308, 939
Vázquez R., López-Martín L., Miranda L. F., Esteban C., Torrelles J. M., Arias L., Raga A. C., 2000, A&A, 357, 1031
Zhang C. Y., Kwok S., 1998, ApJS, 117, 341

This paper has been typeset from a TEX/LATEX file prepared by the author.